Available online at www.sciencedirect.com
SCIENCE DIRECT®
Journal of Sound and Vibration 292 (2006) 583–594
JOURNAL OF SOUND AND VIBRATION
www.elsevier.com/locate/jsvi

Hybrid analytical/numerical method for mode scattering in azimuthally non-uniform ducts

M.C.M. Wright*

Institute of Sound and Vibration Research, University of Southampton, Southampton SO17 1BJ, UK

Received 13 December 2003; received in revised form 5 July 2005; accepted 16 August 2005
Available online 2 November 2005

Abstract

Sound-absorbing liners for ducts are often made in several azimuthal sections with acoustically hard strips, known as splices, between them. These can alter the liner's performance by causing scattering between mode orders, usually to the detriment of overall attenuation. Three-dimensional finite element methods, often involving specialised codes, have previously been used to predict the performance of such spliced liners. Here, an alternative approach is presented which uses a readily available two-dimensional finite element solver to find the modes of the spliced liner and then matches them to the analytical modes of the hard duct. The results are compared with three-dimensional finite element calculations to verify their accuracy. The method as described is for ducts with no flow, but can be extended to flow ducts if necessary.

1. Introduction

Many applications require sound to be attenuated as it travels along an axisymmetric duct without obstructing the duct. Duct liners in which an axial segment of the wall is treated in some way to alter its impedance are widespread and effective in applications ranging from air-conditioning systems to aircraft engines. Manufacturing and maintenance considerations mean that such liners are often made and fitted in a number of azimuthal sections, joined with an acoustically hard strip, referred to hereafter as a splice. The spliced liner usually has less attenuation than a uniform liner with the same impedance, by virtue of the reduced area of liner. A more serious deficiency, however, occurs when high-azimuthal order spinning modes are incident upon the liner. In this case each spinning mode may potentially scatter into other spinning mode of higher- or lower-azimuthal order. This can be a serious problem because liners of this type are typically most effective for modes that are almost cut-off. The modes that are scattered into lower-azimuthal orders can be subjected to significantly less attenuation from the liner than the original input mode. For applications such as aero-engine inlet liners where the liner is designed to attenuate a specific mode generated by the fan, this scattering phenomenon can seriously limit the performance of the liner in respect of its ability to reduce the overall noise level of the device. Evidence for this effect was obtained from engine test measurements by Rademaker et al. [1]. They used a microphone array to decompose the measured sound field into its

*Tel.: +44 23 8059 2291; fax: +44 23 8059 3190.
E-mail address: mcmw@isvr.soton.ac.uk.

0022-460X/$ - see front matter
doi:10.1016/j.jsv.2005.08.011

component modes and found that at certain fan speeds the level of the scattered modes due to a liner with eight splices was significantly higher than that of the rotor-alone tones.

In order to design liners with tolerable splices it is necessary to be able to predict the level and intensity of these scattered tones. One of the first studies of non-uniform liners was made by Lansing and Zorumski [2] who looked at the effects of axial non-uniformity. The problem of azimuthal non-uniformity was studied by Watson [3] and Astley et al. [4] using finite elements. More recently, Regan and Eaton [5] have used finite elements to study spliced liners with input modes of higher-azimuthal orders as computing power has increased.

Watson [6] and Fuller [7,8] used an analytical approach to derive a large system of coupled equations which can, in principle, be solved to obtain the scattering matrix. In practice, however, the numerical effort involved in solving such a large system of equations is likely to be of a similar order to that required to solve the problem numerically by other means. Tester et al. implemented an unpublished approximate formulation by Cargill based on the Kirchoff approximation [9].

The approach described here uses a hybrid analytical–numerical method. The eigenmodes and eigenfrequencies of an infinitely long spliced-lined duct are calculated numerically with a two-dimensional finite element solver. These modes are then matched to the discretised analytical modes of a hard duct to calculate the amplitude of scattered modes for an arbitrary input distribution. Results are presented for a test case which is solved by both this method and by a full three-dimensional finite element calculation, indicating the accuracy of the method. Issues concerning the relative speed of the two methods are described in Section 5. The method as described here is appropriate for ducts without flow, but can be extended to uniform flow cases.

A significant advantage of this method is that it does not require the development of any specialised finite element code. Instead existing Helmholtz solvers can be used. These are widely available and easy to use, meaning that the study of such problems becomes open to those who are not finite element specialists.

2. Theory

2.1. Modal representation

The situation to be considered is shown in Fig. 1 and consists of an infinitely long circular duct of radius a with hard walls. A section of length L is lined with a locally reacting liner that has impedance $Z(\theta)$, which varies azimuthally but not axially. For definiteness it shall be considered to have constant impedance Z everywhere except on two strips $-\Delta/2<\theta<\Delta/2$ and $\pi-\Delta/2<\theta<\pi+\Delta/2$, which are acoustically hard. The method presented can, however, be applied to arbitrary azimuthal variation.

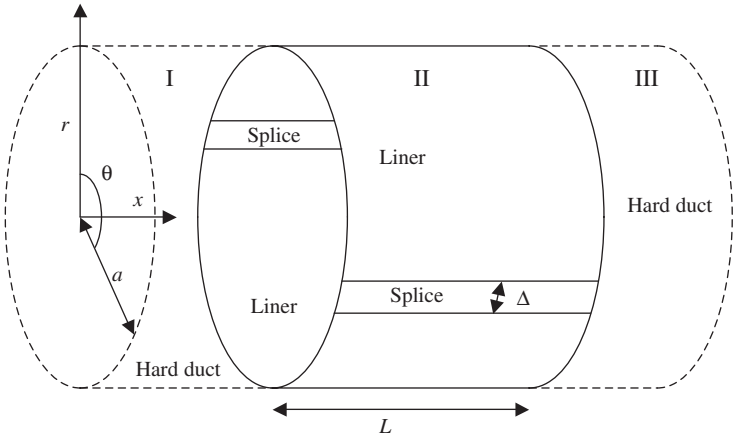

Fig. 1. Schematic diagram of the situation being modelled.

A single time-harmonic spinning mode of the hard-walled duct is incident from $x = -\infty$. It is required to find the amplitudes of the modes reflected towards $x = -\infty$ and of those scattered towards $x = \infty$. Let I, II and III denote the regions to the left of, inside, and to the right of the liner, respectively, as shown on the figure. The pressure field in region I can be written as

$$p^{(I)}(x, r, \theta) = \sum_{m=-\infty}^{\infty} \sum_{n=1}^{\infty} (a^{+}_{m,n} J_m(\kappa_{m,n} r/a) \mathrm{e}^{\mathrm{j}(-k^{I}_{m,n} x + m\theta)} + a^{-}_{m,n} J_m(\kappa_{m,n} r/a) \mathrm{e}^{\mathrm{j}(k^{I}_{m,n} x + m\theta)}), \tag{1}$$

where $\kappa_{m,n}$ is the nth solution of

$$\left. \frac{\mathrm{d}J_m(r)}{\mathrm{d}r} \right|_{r=\kappa_{m,n}} = 0 \tag{2}$$

and $\exp(\mathrm{j}\omega t)$ time-dependence has been suppressed. In region II the pressure field can be written as

$$p^{(II)}(x, r, \theta) = \sum_{n=1}^{\infty} (b^{+} \psi_n \mathrm{e}^{-\mathrm{j}k^{II}_n x} + b^{-} \psi_n \mathrm{e}^{\mathrm{j}k^{II}_n (x+L)}) \tag{3}$$

and in region III it is the same as in region I but with a^{+} and a^{-} replaced by c^{+} and c^{-} and a factor of $\mathrm{e}^{\mathrm{j}kL}$ applied to each term. This means that the a^{+}, a^{-} and b^{+} waves have their origin at $x = 0$ and the b^{-}, c^{+} and c^{-} waves have their origin at $x = L$. The ψ_n in Eq. (3) are the eigenmodes of an infinitely long-lined spliced duct; if they and the corresponding axial wavenumbers k^{II}_n are known then the relationship between the $c^{+}_{m,n}$ and the $a^{+}_{m,n}$ can be estimated by mode-matching. Rather than attempt to find analytic expressions for the transverse eigenmodes of such a duct the approach taken here is to solve the eigenproblem numerically using the finite element method.

2.2. Boundary conditions

The numerical problem is to find approximate solutions to the equation

$$(\nabla^2_{\perp} - \kappa^2_n)\phi_n = 0, \tag{4}$$

where $\nabla^2_{\perp}$ is the two-dimensional Laplacian operator for eigenfunctions ϕ_n (which can be interpreted as velocity potential in this context) over a specified domain with Dirichlet, Neumann or Robin boundary conditions on distinct portions of the boundary.

For the splice regions the boundary condition is

$$\frac{\partial \phi}{\partial n} = 0, \tag{5}$$

that is to say a Neumann boundary condition appropriate to an acoustically hard wall. For the liner the impedance condition is such that

$$p = \rho c u_r Z_{\mathrm{spec}}, \tag{6}$$

where u_r is the normal velocity at the wall, equivalently the radial velocity in a circular duct. Rewriting this equation in terms of velocity potential gives

$$-\rho \mathrm{j}kc\phi = -\rho c \frac{\partial \phi}{\partial n} Z_{\mathrm{spec}} \tag{7}$$

or

$$\phi = \left(\frac{-\mathrm{j}Z_{\mathrm{spec}}}{k} \right) \frac{\partial \phi}{\partial n}. \tag{8}$$

2.3. Mode matching

Let the hard wall modes be numbered according to some scheme so that Eq. (1) can be rewritten as

$$p^{(I)}(x,r,\theta)=\sum_{n=1}^{\infty}(a^{+}\phi_n e^{-jk_n^I x}+a^{-}\phi_n e^{jk_n^I x}). \tag{9}$$

Let $\mathbf{\Phi}$ be a matrix whose columns are the ϕ_n discretised so that each element represents the value at a particular spatial location in (r,θ). These are arranged so that every column of $\mathbf{\Phi}$ corresponds to a particular mode, and every row of $\mathbf{\Phi}$ corresponds to a particular spatial location across the duct cross-section. The dimensions of $\mathbf{\Phi}$ are $N_n \times N_m$, where N_m is the number of modes and N_n is the number of spatial locations. These spatial locations will be the nodes of a finite element decomposition of the domain. Let $\mathbf{a}^+$ be a column vector whose elements are the incident mode amplitudes a_n^+, likewise for $\mathbf{a}^-$, $\mathbf{b}^+$ and so on. Similarly, define $\mathbf{\Psi}$ to be the discretised modes of the lined duct. Approximating the pressure field by a finite number of modes the pressure fields on either side of $x=0$ can be equated by writing

$$\mathbf{\Phi}(\mathbf{a}^{+}+\mathbf{a}^{-})=\mathbf{\Psi}(\mathbf{b}^{+}+\mathbf{E}\mathbf{b}^{-}) \tag{10}$$

and at $x=L$ by writing

$$\mathbf{\Phi}(\mathbf{c}^{+}+\mathbf{c}^{-})=\mathbf{\Psi}(\mathbf{E}\mathbf{b}^{+}+\mathbf{b}^{-}), \tag{11}$$

where $\mathbf{E}$ is a diagonal matrix whose nth element is $e^{jk_n^{II}L}$. In a similar manner, axial velocity can be matched by writing

$$\mathbf{\Phi}\mathbf{K}^h(\mathbf{a}^{+}-\mathbf{a}^{-})=\mathbf{\Psi}\mathbf{K}^l(\mathbf{b}^{+}-\mathbf{E}\mathbf{b}^{-}) \tag{12}$$

and

$$\mathbf{\Phi}\mathbf{K}^h(\mathbf{c}^{+}-\mathbf{c}^{-})=\mathbf{\Psi}\mathbf{K}^l(\mathbf{E}\mathbf{b}^{+}-\mathbf{b}^{-}), \tag{13}$$

where $\mathbf{K}^h$ is a diagonal matrix whose nth element is k_n^I, the wavenumbers for the hard-walled duct, and $\mathbf{K}^l$ is a diagonal matrix whose nth element is k_n^{II}, the wavenumbers for the lined duct.

Eqs. (10) and (12) can be combined as

$$\begin{pmatrix}\mathbf{\Phi} & \mathbf{\Phi}\\ \mathbf{\Phi}\mathbf{K}^h & -\mathbf{\Phi}\mathbf{K}^h\end{pmatrix}\begin{pmatrix}\mathbf{a}^{+}\\ \mathbf{a}^{-}\end{pmatrix}=\begin{pmatrix}\mathbf{\Psi} & \mathbf{\Psi}\mathbf{E}\\ \mathbf{\Psi}\mathbf{K}^l & -\mathbf{\Psi}\mathbf{K}^l\mathbf{E}\end{pmatrix}\begin{pmatrix}\mathbf{b}^{+}\\ \mathbf{b}^{-}\end{pmatrix}, \tag{14}$$

while Eqs. (11) and (13) give

$$\begin{pmatrix}\mathbf{\Phi} & \mathbf{\Phi}\\ \mathbf{\Phi}\mathbf{K}^h & -\mathbf{\Phi}\mathbf{K}^h\end{pmatrix}\begin{pmatrix}\mathbf{c}^{+}\\ \mathbf{c}^{-}\end{pmatrix}=\begin{pmatrix}\mathbf{\Psi}\mathbf{E} & \mathbf{\Psi}\\ \mathbf{\Psi}\mathbf{K}^l\mathbf{E} & -\mathbf{\Psi}\mathbf{K}^l\end{pmatrix}\begin{pmatrix}\mathbf{b}^{+}\\ \mathbf{b}^{-}\end{pmatrix}. \tag{15}$$

In the present problem $\mathbf{a}^+$ is specified, $\mathbf{c}^-=\mathbf{0}$ to satisfy the usual radiation condition, and $\mathbf{c}^+$ is required. Further rearranging gives

$$\begin{pmatrix}\mathbf{\Phi} & -\mathbf{\Psi}\mathbf{E}\\ \mathbf{\Phi}\mathbf{K}^h & -\mathbf{\Psi}\mathbf{K}^l\mathbf{E}\end{pmatrix}\begin{pmatrix}\mathbf{a}^{+}\\ \mathbf{b}^{-}\end{pmatrix}=\begin{pmatrix}\mathbf{\Psi} & -\mathbf{\Phi}\\ \mathbf{\Psi}\mathbf{K}^l & \mathbf{\Phi}\mathbf{K}^h\end{pmatrix}\begin{pmatrix}\mathbf{b}^{+}\\ \mathbf{a}^{-}\end{pmatrix} \tag{16}$$

and

$$\begin{pmatrix}\mathbf{\Psi}\mathbf{E} & -\mathbf{\Phi}\\ \mathbf{\Psi}\mathbf{K}^l\mathbf{E} & \mathbf{\Phi}\mathbf{K}^h\end{pmatrix}\begin{pmatrix}\mathbf{b}^{+}\\ \mathbf{c}^{-}\end{pmatrix}=\begin{pmatrix}\mathbf{\Phi} & -\mathbf{\Psi}\\ \mathbf{\Phi}\mathbf{K}^h & \mathbf{\Psi}\mathbf{K}^l\end{pmatrix}\begin{pmatrix}\mathbf{c}^{+}\\ \mathbf{b}^{-}\end{pmatrix}. \tag{17}$$

In principle, this system of equations can be solved to give $\mathbf{c}^+$ in terms of $\mathbf{a}^+$ but in practice this approach suffers from poor conditioning. The following alternative approach has been found to be successful in such cases [10].

1. Set $\mathbf{b}^-=\mathbf{0}$ in Eq. (16).
2. Solve Eq. (16) for $\mathbf{b}^+$ and $\mathbf{a}^-$.

3. Use the resulting $\mathbf{b}^+$ in Eq. (17) and solve for $\mathbf{c}^+$ and $\mathbf{b}^-$.
4. Repeat steps 2–4 but use the values for $\mathbf{b}^-$ calculated in the previous iteration instead of zero.

The procedure as described above imposes a matching condition at every node of the discretised cross-section. This leads to very large, non-square, matrices in Eqs. (16), (17) and relatively poor results since no spatial averaging occurs. It also requires two over-determined systems of equations to be solved in each iteration, since the number of nodes will typically be much larger than the number of modes. Better results can be achieved by projecting the matching condition onto a set of basis functions such as the hard-wall modes, and by using the mass-matrix of the finite element mesh to average across elements. This can be implemented by following the same procedure as described above but premultiplying every element in the matrices in Eqs. (16) and (17) by $\mathbf{\Phi M}$, where $\mathbf{M}$ is the mass matrix. This also reduces the size of the matrices in Eqs. (16) and (17) from $2N_n \times (N_m^I + N_m^{II})$ to $2N_m \times (N_m^I + N_m^{II})$, where N_n is the number of nodes in the mesh and the N_m are the number of modes included in each region. Furthermore, if N_m^I and N_m^{II} are chosen to be equal the resulting matrices will be square, allowing simpler, more efficient solution techniques. This procedure converges to a stable answer that is typically to within 0.1 dB within five iterations.

In order to accurately represent the field across the matching region N_m^I should be chosen so that all cut-on and a few cut-off modes are included, and N_m^{II} should be chosen to be sufficiently large that the largest real part of a tranvserse wavenumber for the lined section modes is close to the highest transverse wavenumber of the hard wall modes. The cut-off modes in region I will evanesce in the axial direction but oscillate in the transverse plane so it is necessary to discretise the cross-section sufficiently finely that such transverse pressure patterns can still be adequately represented.

The method as presented above finds the transmitted and reflected modal amplitudes for one particular incident field, which has a single corresponding modal amplitude vector $\mathbf{a}^+$. Once $\mathbf{\Psi}$ has been found, however, it is simple to determine the transmitted and reflected response to *any* input field by replacing $\mathbf{a}^+$ with the identity matrix and letting all the other modal amplitude vectors become matrices of the same width. The matrices that are then found corresponding to what were $\mathbf{c}^+$ and $\mathbf{a}^-$ will consist of columns each of which gives the scattered and reflected modal amplitudes for each unit amplitude incident mode. With this the response to any incident wavefield can be synthesised.

At any stage of the matching process the pressure mismatch at each of the interfaces can be examined by evaluating $\mathbf{\Phi}(\mathbf{a}^+ + \mathbf{a}^-) - \mathbf{\Psi}(\mathbf{b}^+ + \mathbf{E}\mathbf{b}^-)$ for the entrance and $\mathbf{\Psi}(\mathbf{E}\mathbf{b}^+ + \mathbf{b}^-) - \mathbf{\Phi}(\mathbf{c}^+ + \mathbf{c}^-)$ for the exit to the liner. In this way the size and distribution of any error can be assessed.

3. Test cases

3.1. Comparison with specialised finite element software

A test case was defined in which the liner length L was equal to a the radius of the duct and the frequency was such that $ka = 12.948$. This value was chosen so that the mode with $m = 10$ and $n = 1$ is 10% cut on, that is to say $ka = 1.1 \times \kappa_{10,1}$. Two cases for the specific impedance of the liner were chosen, one with $Z_{\text{spec}} = 2 - \text{j}$ and one with $Z_{\text{spec}} = 2 + \text{j}$. Both signs were chosen because it has been shown by Rienstra [11] that modal characteristics are quite different in the two cases, with a distinct family of 'surface modes' being exhibited in one case. By exploring both cases it was possible to verify that the procedure works in both cases. The liner contained two splices, diametrically opposite each other. Each splice had a width $\Delta = 7.72$ cm (measured as the length of the arc it made around the duct) so that non-dimensional splice width $k\Delta = 1$. This meant that the angle subtended by each splice was $\Delta = 0.0772$ radians or 4.425°.

Having two equally spaced, equally sized splices means that the problem is symmetrical and could be reduced to a smaller problem. In this test, however, the full problem was solved. The symmetry means that only modes whose azimuthal order differs from that of the incident mode by an even number will be excited. By using both procedures to predict the amplitude of all modes, not just those that will be excited it is possible to assess the noise floor of the method by determining the predicted level of modes whose amplitude should be non-existent.

The eigenvalue solver used was that incorporated into the MATLAB partial differential equations toolbox [12]. The matching was performed in MATLAB, and the resulting systems of equations were solved using MATLAB's '\' operator in each iteration.

A single mode of azimuthal order $m = 10$ and radial order $n = 1$, with an amplitude of 150 dB was incident from the left, i.e. $a^{+}_{10,1} = 894.42$ in Eq. (1). The procedure described above with ten iterations of the matching procedure were used to calculate the amplitudes of the modes scattered and transmitted to the other side of the liner, i.e. the values of $\mathbf{c}^{+}$. For comparison the same problem was solved using a full three-dimensional model implemented using the ACTRAN finite element package [13], which allows inputs and outputs to models to be specified in terms of hard-wall duct mode amplitudes. The mesh for the ACTRAN model also had ten nodes per wavelength, details of the meshing procedure are given in Refs. [14,15].

3.2. Reactive liner energy budget

A second test case was carried out in which the impedance of the lined section was made purely reactive, that is to say with Z_{spec} purely imaginary. Under these circumstances there is no energy loss mechanism within the liner, so the transmitted and reflected energies ought to add up to the incident energy. Both positive and negative reactances were tested, and both single mode and multiple mode inputs were used. No special procedures had to be employed with regard to mode ordering.

4. Results

4.1. Comparison with specialised finite element software

Fig. 2 shows the spectrum of complex values of k_n^{II} obtained for the spliced lined duct with $Z_{\text{spec}} = 2 + \text{j}$. Fig. 3 shows the corresponding spectrum for the case when $Z_{\text{spec}} = 2 - \text{j}$. The family of points corresponding

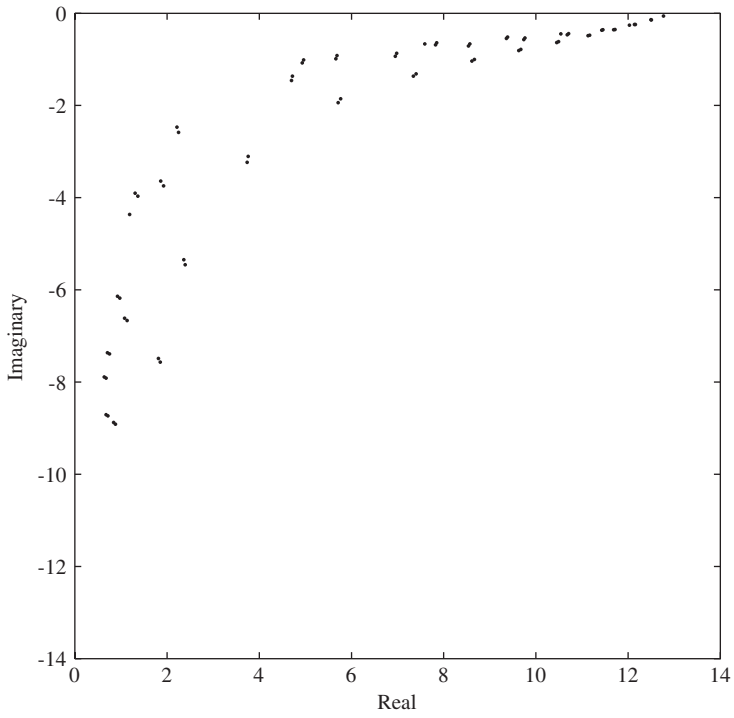

Fig. 2. Spectrum of complex values of k_n^{II} for the spliced duct with $Z_{\text{spec}} = 2 + \text{j}$.

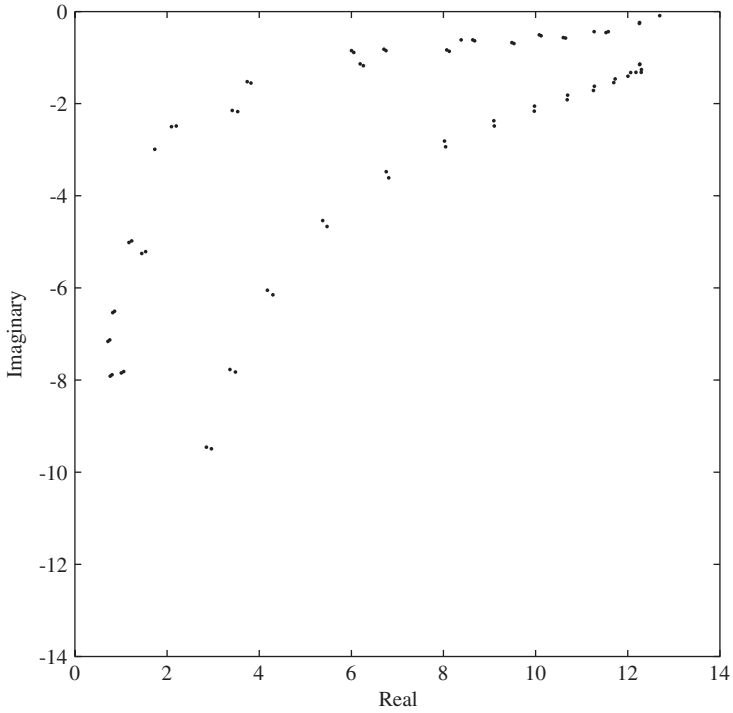

Fig. 3. Spectrum of complex values of k_n^{II} for spliced duct with $Z_{\text{spec}} = 2 - \text{j}$.

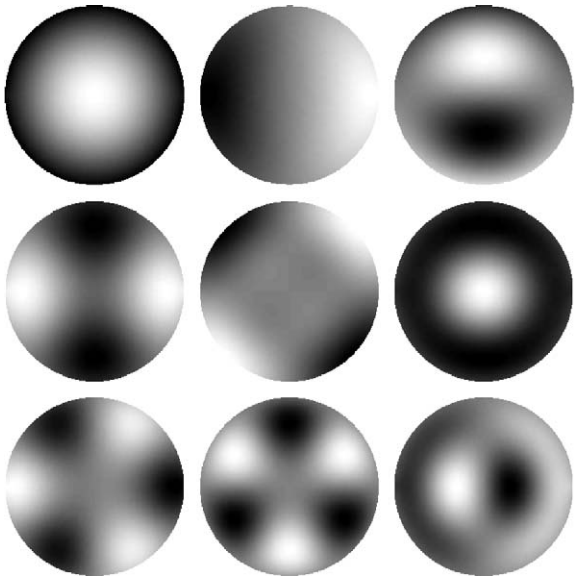

Fig. 4. A selection of modeshapes for the spliced duct with $Z_{\text{spec}} = 2 + \text{j}$.

to the surface waves are seen as a separate family further from the origin than the ordinary modes. In both cases the points occur in pairs that are very close. This is not a result of numerical error, unlike the azimuthally uniform duct in which the eigenvalues occur in pairs, here the symmetry is broken by the splices which causes the eigenvalue pairs to separate. This issue is further examined below.

Fig. 4 shows nine sample modeshapes for the case when $Z_{\text{spec}} = 2 + \text{j}$. These are the modes with the lowest real parts of their transverse wavenumber, and hence the highest real part of k_n^{II}. Only the real part of the

complex modeshape is displayed. The departure from modes of the equivalent unspliced lined duct is hard to see, though it can be detected with a fine enough amplitude scale. Fig. 5 shows nine sample modeshapes for the case when $Z_{\text{spec}} = 2 - \text{j}$. The 4th, 5th, 7th and 9th modeshapes (reading from left to right) correspond to

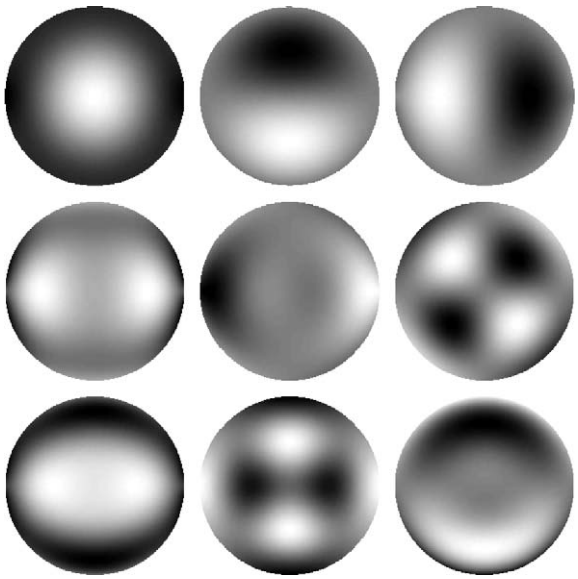

Fig. 5. A selection of modeshapes for the spliced duct with $Z_{\text{spec}} = 2 - \text{j}$.

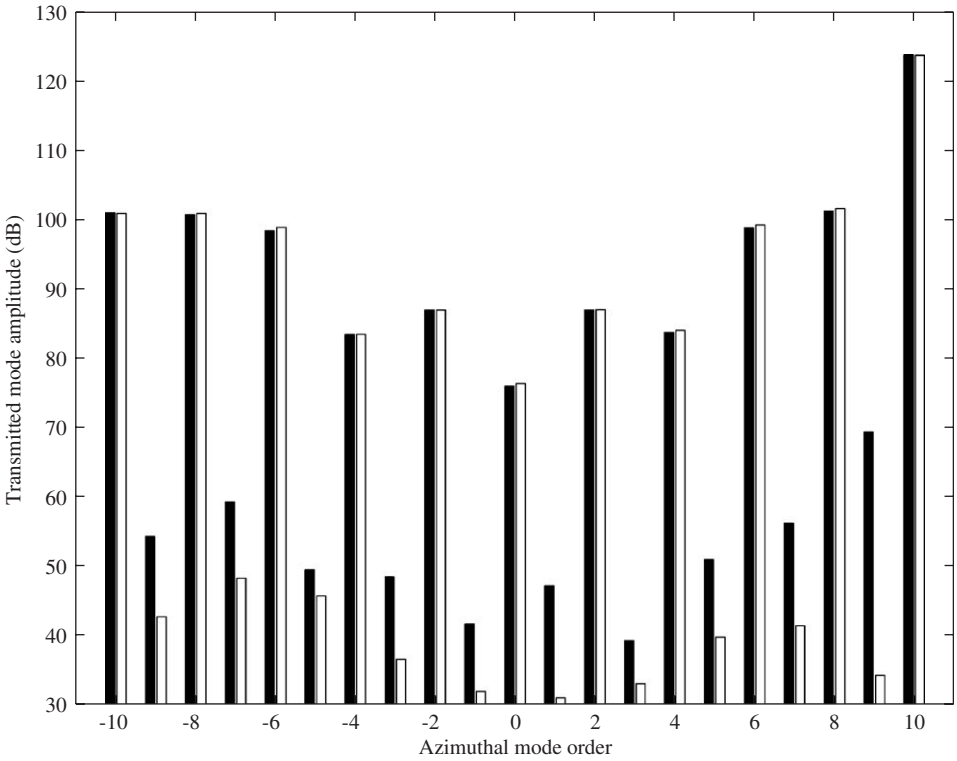

Fig. 6. Comparison of transmitted mode amplitudes (dB) with radial order $n = 1$ for the case $Z_{\text{spec}} = 2 + \text{j}$, calculated by three-dimensional finite elements (light) and two-dimensional mode matching (dark).

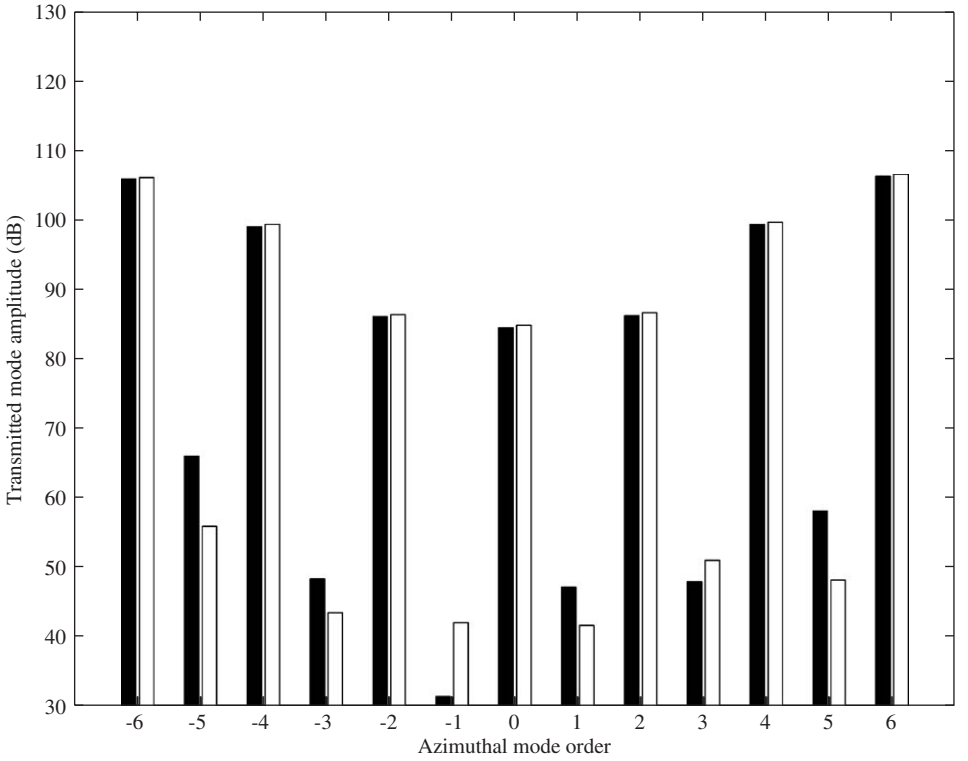

Fig. 7. Comparison of transmitted mode amplitudes (dB) with radial order $n = 2$ for the case $Z_{\text{spec}} = 2 + \text{j}$, calculated by three-dimensional finite elements (light) and two-dimensional mode matching (dark).

surface waves and have corresponding values of k_n^{II} lying on the branch that is further from the origin than the ordinary modes. It is noticeable that these modes seem to show the effect of the splice more pronouncedly.

Fig. 6 shows the amplitudes of the scattered modes with radial order $n = 1$ for the case where $Z_{\text{spec}} = 2 + \text{j}$. The higher amplitudes for the mode-matched results in the odd azimuthal orders indicates that a higher noise level was obtained using the two-dimensional method, since in principle these amplitudes should be $-\infty$ dB. The modes that are really scattered show an agreement to within 0.5 dB and this agreement can be improved if necessary by increasing resolution, at the expense of computation time. Fig. 7 shows a similar level of agreement for the radial order $n = 2$, and indeed similar agreement is obtained for the entire population of cut-on modes, though the rest are not shown to save space. Figs. 8 and 9 show similar agreement for the case when $Z_{\text{spec}} = 2 - \text{j}$, indicating that ducts which bear surface waves can be treated just as well by this method as those that do not.

The time taken by the mode-matching procedure was approximately 20 min, using a 1 GHz PC with 1 Gbyte of RAM. Most of the time was taken in automatic generation of the mesh and calculation of the modes. The mode matching procedure and the calculation of the hard-wall modes took less than a minute. A compiled eigenvalue solver using library functions took less than half this time. The time taken by ACTRAN to produce the corresponding results was approximately 30 min on the same platform. This did not include the time taken to generate the mesh which was done by hand using the ICEMCFD package.

4.2. Reactive liner energy budget

The energy of each transmitted mode was calculated from

$$W_{m,n} = \frac{\pi k_{m,n}^{III}}{k}\left[a^2 - \left(\frac{m}{\kappa_{m,n}}\right)^2\right]\frac{J_m^2(\kappa_{m,n}a)|c_{m,n}^{+}|^2}{2\rho c} \tag{18}$$

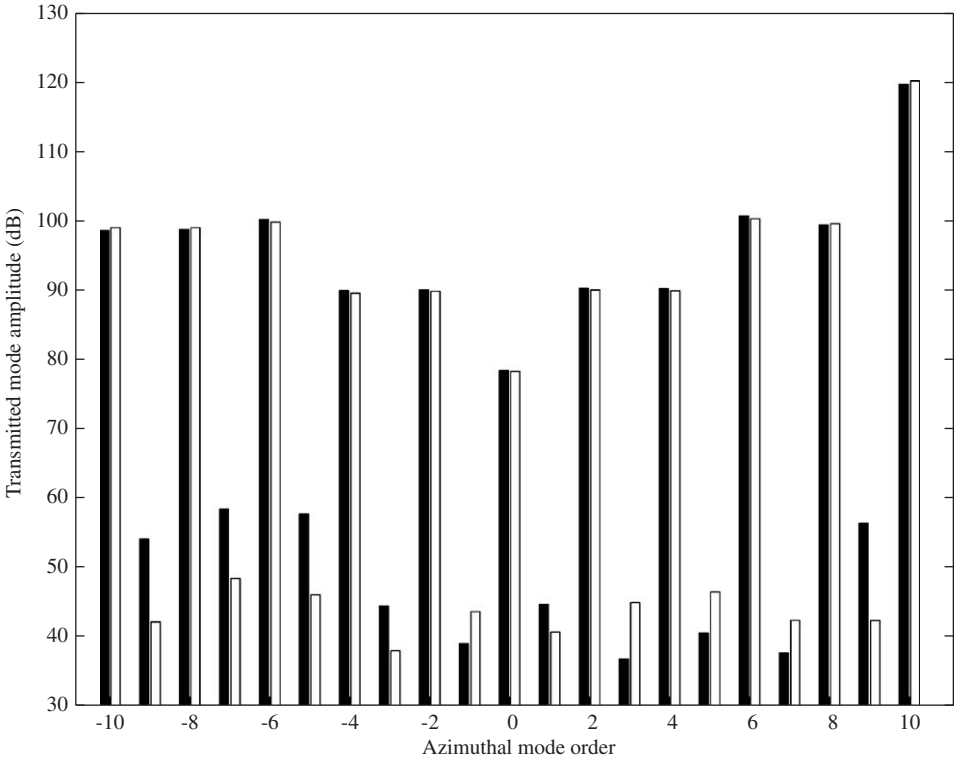

Fig. 8. Comparison of transmitted mode amplitudes (dB) with radial order $n = 1$ for the case $Z_{\text{spec}} = 2 - \text{j}$, calculated by three-dimensional finite elements (light) and two-dimensional mode matching (dark).

and similarly for the reflected modes with $k^{I}_{m,n}$ and $a^{-}_{m,n}$ instead of $k^{III}_{m,n}$ and $c^{+}_{m,n}$. In every case the spurious loss

$$L_{\text{error}} = 10\log_{10}\left(\frac{W_{\text{input}} - W_{\text{transmitted}} - W_{\text{reflected}}}{W_{\text{input}}}\right) \tag{19}$$

was found to be less than -75 dB with sufficient resolution of the finite element mesh. Each individual modal amplitude also agreed with results from ACTRAN but these are not presented in full for reasons of space. Multi-modal inputs were handled with no special provisions.

The only case that needs a little care is for purely reactive liners with small negative reactance. In these cases, as Rienstra has shown [11], a complex solution exists despite the fact that the boundary conditions for the associated two-dimensional Helmholtz problem are real. For some commercial solvers it is necessary to explicitly alert them to the possible presence of such solutions.

5. Discussion

It has been demonstrated that matching modes obtained from a two-dimensional finite element model provides an alternative to solving a three-dimensional finite element model for this type of problem. The question of which method is preferable depends on circumstances, the deciding factors being accuracy of solution and time of execution. As has been shown the two methods produce similar results but since there are no analytic benchmarks available for this problem it is not possible to say which is more accurate. It is, however, possible to predict situations where each method will have an advantage because the computation time of the two-dimensional method is independent of the axial length of the lined section of the duct, whereas the three-dimensional model size will increase proportionately with this length. Therefore, it is reasonable to assume that for sufficiently long liners the two-dimensional method will be faster. Furthermore, once a representative set of modes for a particular Helmholtz number have been obtained it is a trivial matter to solve

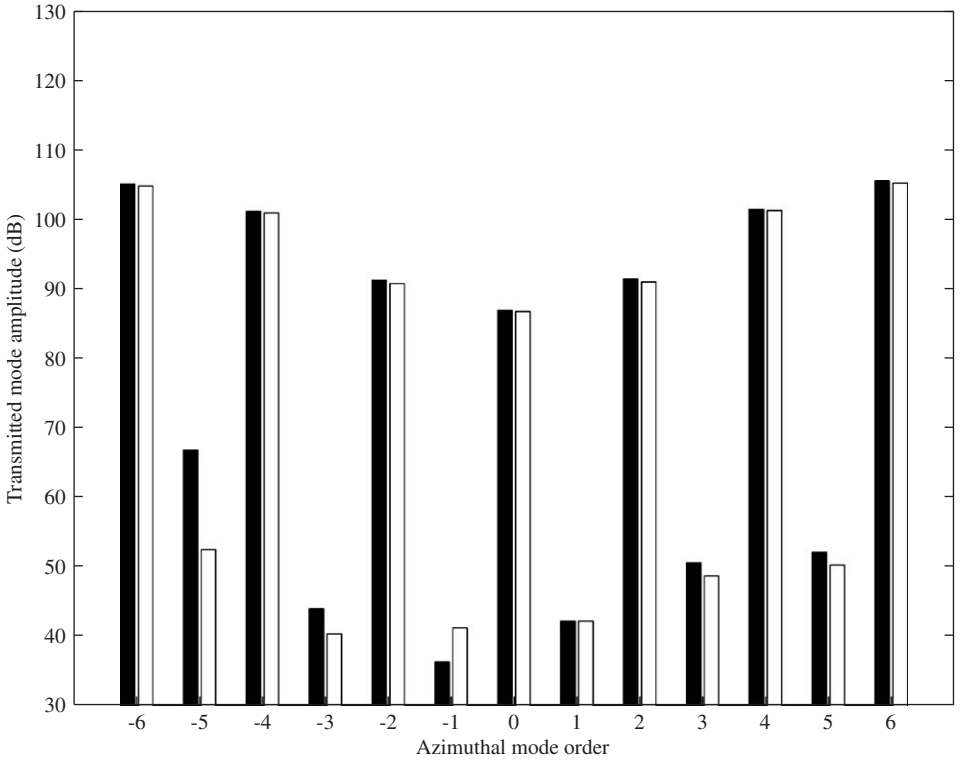

Fig. 9. Comparison of transmitted mode amplitudes (dB) with radial order $n = 2$ for the case $Z_{\text{spec}} = 2 - \text{j}$, calculated by three-dimensional finite elements (light) and two-dimensional mode matching (dark).

further transmission problems since the modes do not need to be recalculated each time. For both methods the computation time could be reduced by exploiting the symmetry of the problem. In the case considered here it would be necessary to consider only half the duct (cut either midway through the splices or midway through the lined sections). By calculating modes with Dirichlet conditions and then Neumann conditions on the cut boundary it would be possible to obtain all modes for the full problem. The matching could also be applied to this half-problem as well if desired.

For simulations of realistic aircraft liner conditions it would be desirable to incorporate the effect of flow, and this capability is already present in the ACTRAN package. The two-dimensional method described here could be extended to solve the same problem in the presence of uniform flow with a purpose-written solver. In this case the modeshapes in the lined section would be different for modes propagating upstream and downstream so the finite element problem to be solved would be larger. One approach would be to use the ordinary Helmholtz solver to solve each class of modes as a separate problem. This would require an equivalent boundary condition to be obtained using the procedure due to Ingard [16]. Unfortunately, this results in a boundary condition that depends on the eigenvalue to be obtained. It is possible to solve such problems with a standard Helmholtz solver, by using the no-flow eigenvalue as an initial value and then iterating until the correct solution is obtained. Unfortunately this procedure has to be followed for each individual mode. It is therefore considerably more efficient to solve the coupled implicit-eigenvalue two-dimensional problem as can be done using, for example, the FEMLAB package. This restricts the choice of solver but is not greatly more complicated in principle than the method as described.

Acknowledgements

This work was supported by the Rolls–Royce University Technology Centre in Gas Turbine Noise at the ISVR. The author gratefully acknowledges the assistance of R.J. Astley, A. McAlpine and V. Hii.

References

[1] E. Rademaker, P. Sijtsma, B.J. Tester, Mode detection with an optimised array in a model turbofan engine intake at varying shaft speeds, in: *Seventh AIAA/CEAS Aeroacoustics Conference*, No. AIAA-2001-2181, 2001.
[2] D.L. Lansing, W.E. Zorumski, Effects of wall admittance changes on duct transmission and radiation of sound, *Journal of Sound and Vibration* 27 (1) (1973) 85–100.
[3] W. Watson, A finite element simulation of sound attenuation in a finite duct with a peripherally variable liner, Technical Report TM-74080, NASA, 1977.
[4] R.J. Astley, N. Walkington, W. Eversman, Transmission in flow ducts with peripherally varying liner, in: *AIAA Conference Paper*, No. AIAA-80-1015, 1980.
[5] B. Regan, J. Eaton, Modelling the influence of acoustic liner nonuniformities on duct modes, *Journal of Sound and Vibration* 219 (5) (1999) 859–879.
[6] W. Watson, Noise suppression characteristics of peripherally segmented duct liners, Technical Report TP-1904, NASA, 1981.
[7] C.R. Fuller, Propagation and radiation of sound from flanged circular ducts with circumferentially varying wall admittances, I: semi-infinite ducts, *Journal of Sound and Vibration* 93 (3) (1984) 321–340.
[8] C.R. Fuller, Propagation and radiation of sound from flanged circular ducts with circumferentially varying wall admittances, II: finite ducts with sources, *Journal of Sound and Vibration* 93 (3) (1984) 341–351.
[9] B.J. Tester, N. Baker, A. Kempton, M.C.M. Wright, Validation of an analytical model for scattering by intake liner splices, in: *10th AIAA/CEAS Aeroacoustics Conference*, No. AIAA-2004-2906, 2004.
[10] A. Cummings, High frequency ray acoustics models for duct silencers, *Journal of Sound and Vibration* 221 (4) (1999) 681–708.
[11] S.W. Rienstra, A classification of duct modes based on surface waves, *Wave Motion* 37 (2) (2003) 119–135.
[12] The Mathworks, *Partial Differential Equation Toolbox for Use with MATLAB*, The Mathworks, Natick, MA, 1996.
[13] Free Field Technologies, *Actran 2003 Users' Guide*, Free Field Technologies, 2003 http://www.fft.be.
[14] A. McAlpine, M.C.M. Wright, S. Thezelais, H. Batard, Finite/boundary element assessment of a turbofan spliced intake liner at supersonic operating conditions, in: *Ninth AIAA/CEAS Aeroacoustics Conference*, No. AIAA-2003-3305, 2003.
[15] A. McAlpine, M.C.M. Wright, Acoustic scattering by a spliced turbofan inlet duct liner at supersonic fan speeds, *Journal of Sound and Vibration*, 2005, in press.
[16] U. Ingard, Influence of fluid motion past a plane boundary on sound reflection, absorption and transmission, *Journal of the Acoustical Society of America* 31 (7) (1959) 1035–1036.